Supporting Information (SI)

Asymmetric [Ir(C_1^N_1)(C_2^N_2)(L^X)]-*Tris*-Heteroleptic Iridium(III) Complexes Enable Deep Blue Phosphorescent Emission

Li Gu, [a,] *Shuaibing Li,* [c] *Huabo Han,* [e] *Xinzhong Wang,* [a] *Changjiang Zhou,* [d] *Junjian Lu,* [b,*] *Liang Zhou,* [c,*] *Guangzhao Lu* [a,*]

[a] Shenzhen Institute of Information Technology, Shenzhen, 518172, China.

[b] Hunan Provincial Key Laboratory of Fine Ceramics and Powder Materials, Advanced Ceramic Modern Industry College, Hunan University of Humanities, Science and Technology, Loudi 417000, China.

[c] State Key Laboratory of Rare Earth Resource Utilization, Changchun Institute of Applied Chemistry, Chinese Academy of Sciences, Changchun 130022, China.

[d] College of Chemical Engineering, Zhejiang University of Technology, Hangzhou 310014, China.

[e] College of Chemistry and Chemical Engineering, Shangqiu Normal University, Shangqiu 476000, China

E-mail: lugz@sziit.edu.cn; lujunjian2001@126.com; zhoul@ciac.ac.cn.

Table of Contents

Materials and Measurements

All reagents and chemicals were purchased from commercial sources and used without further purification. ^{1}H NMR spectra were recorded by Bruker Advanced II (400 MHz) spectrometers and MERCURYVX300 using CD_2Cl_2 as solvent and tetramethylsilane (TMS) as the internal standards. High resolution mass spectra (HRMS) were measured by Thermo Scientific LTQ Orbitrap XL mass spectrometer. Thermo gravimetric analyses (TGAs) were performed on a NETZSCH STA 449C instrument under nitrogen with a heating rate of 10 $^{o}C\ min^{-1}$. Elemental analyses for C, H, and N were performed on an Elementar Vario MICRO analyzer. The absorption and photoluminescence spectra were measured on a Shimadzu UV-2700 recording spectrophotometer and a Hitachi F-4600 photoluminescence spectrophotometer, respectively. The decay lifetimes were performed on PicoQuant Fluotime300 in degassed CH_2Cl_2 solution at room temperature. Absolute PLQYs in degassed CH_2Cl_2 solution were obtained using a Quantaurus-QY measurement system (C9920-02, Hamamatsu Photonics).

Synthesis of Ligands and Iridium Complexes

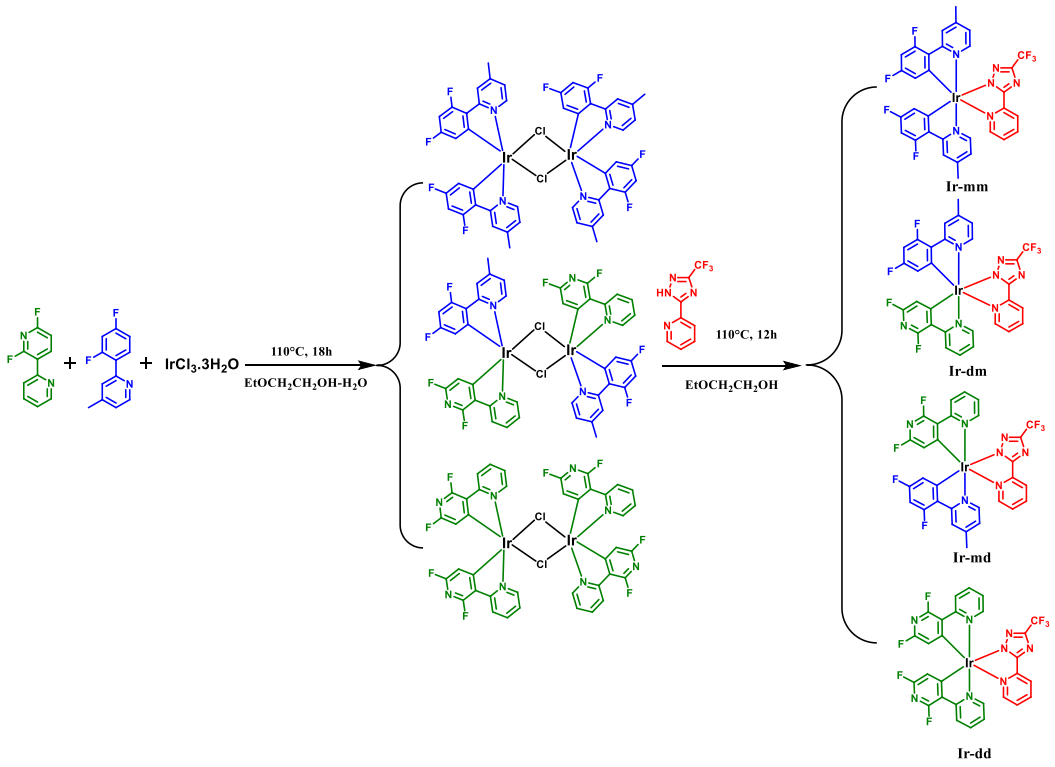

Scheme S1 The synthetic routes of the Ir(III) complexes.

The two main ligands of dfbpy (2',6'-difluoro-2,3'-bipyridine) and medfppy (2-(2,4-difluorophenyl)-4-methylpyridine) were synthesized by the Suzuki coupling reaction, and the ancillary ligand of fptz (2-(3-(trifluoromethyl)-1*H*-1,2,4-triazol-5-yl)pyridine) is available through commercialization.

To a stirred solution of the equimolar amount of the ligands of dfbpy (211 mg, 1.1 mmol) and medfppy (225 mg, 1.1 mmol) in 2-ethoxyethanol/H_2O (16 mL; 3:1 (v/v)), $IrCl_3$ $3H_2O$ (352 mg, 1.0 mmol) was added, the resultant mixture was heated to 110 ℃ and continuously stirred under a N_2 atmosphere for 18 h. After cooling to room temperature, the water (30 mL) was added, and the formed μ-chloro-bridged dimer intermediates containing $[Ir(dfbpy)(medfppy)(\mu\text{-}Cl)]_2$, $[Ir(medfppy)_2(\mu\text{-}Cl)]_2$ and $[Ir(dfbpy)_2(\mu\text{-}Cl)]_2$ were collected by filtration. Subsequently, after drying, the μ-chloro-bridged dimer intermediates (1.0 equiv.), Na_2CO_3 (2.4 equiv.) and fptz (2.4 equiv.) were added to 2-ethoxyethanol (30 mL), and the reaction mixture was

continuously refluxed under a N_2 atmosphere for another 12 h. After dryness under vacuum, the residue was extracted with CH_2Cl_2, and the combined organic phase was dried over anhydrous Na_2SO_4. The solvent was removed under reduced pressure, and the residue was further purified by silica gel column chromatography with CH_2Cl_2/EtOAc (20 : 1; v/v) as the eluent, affording the desirable product and the by-products, respectively. Four final products Ir(medfppy)$_2$(fptz) (Ir-mm**)**, Ir(dfbpy)(medfppy)(fptz) (Ir-dm**)**, Ir(medfppy)(dfbpy)(fptz) (Ir-md**)** and Ir(dfbpy)$_2$(fptz) (Ir-dd**)** were obtained simultaneously. Owing to the poor sublimation result of Ir-dd, it was not been further investigated in detail.

For the first eluted Ir(medfppy)$_2$(fptz) (Ir-mm**)**: Yield: 10%. ^{1}H NMR (400 MHz, Methylene Chloride-d_2) δ 8.42 (t, J = 7.6 Hz, 1H), 8.10 (s, 1H), 8.05 (s, 1H), 7.95-7.91 (m, 1H), 7.76 (d, J = 5.5 Hz, 1H), 7.47 (d, J = 6.0 Hz, 1H), 7.29-7.22 (m, 2H), 6.83-6.81 (m, 1H), 6.77-6.75 (m, 1H), 6.54-6.44 (m, 2H), 5.81 (d, J = 10.9 Hz, 1H), 5.73 (d, J = 11.1 Hz, 1H), 2.48 (s, 3H), 2.46 (s, 3H). HR-MS, m/z: calcd for $C_{32}H_{21}F_7N_6Ir^+$ $[M+H]^+$ 815.1345, found 815.1342. Anal. Calcd for $C_{32}H_{20}F_7IrN_6$: C, 47.23; H, 2.48; N, 10.33. Found: C, 46.89; H, 2.63; N, 10.74%.

For the second eluted Ir(dfbpy)(medfppy)(fptz) (Ir-dm**)**: Yield: 19%. ^{1}H NMR (400 MHz, Methylene Chloride-d_2) δ 8.30-8.18 (m, 2H), 8.12 (d, J = 1.7 Hz, 1H), 7.93 (td, J = 7.8, 1.6 Hz, 1H), 7.85-7.78 (m, 1H), 7.76 (ddd, J = 5.5, 1.5, 0.9 Hz, 1H), 7.67 (ddd, J = 5.8, 1.6, 0.7 Hz, 1H), 7.29 (d, J = 6.0 Hz, 1H), 7.23 (ddd, J = 7.6, 5.5, 1.4 Hz, 1H), 7.12-7.01 (m, 1H), 6.79 (dd, J = 6.0, 1.6 Hz, 1H), 6.50 (ddd, J = 12.7, 9.2, 2.4 Hz, 1H), 5.87 (t, J = 2.1 Hz, 1H), 5.65 (dd, J = 8.5, 2.4 Hz, 1H), 2.49 (s, 3H). HR-MS, m/z: calcd for $C_{30}H_{18}F_7N_7Ir^+$ $[M+H]^+$ 802.1141, found 802.1140. Anal. Calcd for $C_{30}H_{17}F_7IrN_7$: C, 45.00; H, 2.14; N, 12.25. Found: C, 45.43; H, 2.36; N, 12.68%.

For the third eluted Ir(medfppy)(dfbpy)(fptz) (Ir-md**)**: Yield: 15%. ^{1}H NMR (400 MHz, Methylene Chloride-d_2) δ 8.31-8.19 (m, 2H), 8.06 (s, 1H), 7.93 (td, J = 7.8, 1.6 Hz, 1H), 7.86-7.78 (m, 1H), 7.75 (ddd, J = 5.5, 1.5, 0.8 Hz, 1H), 7.51 (ddd, J = 5.8,

1.5, 0.7 Hz, 1H), 7.46 (d, *J* = 6.0 Hz, 1H), 7.24 (ddd, *J* = 7.5, 5.5, 1.4 Hz, 1H), 7.00 (ddd, *J* = 7.4, 5.8, 1.4 Hz, 1H), 6.89-6.81 (m, 1H), 6.54 (ddd, *J* = 12.5, 9.2, 2.4 Hz, 1H), 5.80-5.71 (m, 2H), 2.48 (s, 3H). HR-MS, m/z: calcd for $C_{30}H_{18}F_7N_7Ir^+$ $[M+H]^+$ 802.1141, found 802.1142. Anal. Calcd for $C_{30}H_{17}F_7IrN_7$: C, 45.00; H, 2.14; N, 12.25. Found: C, 45.39; H, 2.38; N, 12.65%.

X-ray Crystallography

The single crystals of the two complexes were obtained from slow evaporation of methanol/CH_2Cl_2 solution at room temperature. And its X-ray-diffraction data were carried out on a Bruker APEX2 SMART CCD diffractometer at room temperature. Cell parameters were retrieved using SMART software and refined using SAINT on all observed reflections. Data were collected using a narrow-frame method with scan widths of 0.30 ° in ω and an exposure time of 10 s/frame. Crystal structures were solved by direct methods using the SHELXL-2014/7' software. None-hydrogen atoms were refined anisotropically by full-matrix least-squares calculations on F^2 using SHELXL-2014/7', while the hydrogen atoms were directly introduced at calculated position and refined in the riding mode.

Cyclic Voltammetry Measurements and Theoretical Calculations

Cyclic voltammetry (CV) was measured on a CHI voltammetric analyzer at room temperature with the conventional three-electrode configuration, consisted of a platinum column working electrode, a platinum wire auxiliary electrode, and an Ag wire pseudo reference electrode. Cyclic voltammograms were recorded using tetrabutylammonium hexafluorophosphate (TBAPF6) (0.1 M) dissolved in dichloromethane (5 mL) as the supporting electrolyte, and ferrocenium-ferrocene (Fc^+/Fc) as the external standard, at the scan rate of 100 mV s^{-1}. The onset potential was determined from the intersection of two tangents of the rising and background current in cyclic voltammogram. To gain further insight into the photophysical and

electrochemical characteristics of the Ir(III)-complexes, theoretical studies on their electronic structures were carried out by using density functional theory (DFT) and time-dependent DFT (TD-DFT) methods. Each of their molecular structures was optimized at the ground state (S_0) in the gas phase. DFT calculations were conducted with the popular B3LYP functional theory. The 6-31G (d,p) basis set was applied for C, H, N and F atoms, while effective core potentials employed for Ir atom were based on a LanL2DZ basis set. The energies of the excited states of the Ir(III) complex were computed by TD-DFT based on all the ground-state (S_0) geometries. Additionally, the natural transition orbital (NTO) was analyzed for $S_0 \rightarrow T_1$ excitation based on the first triplet state (T_1) geometries optimized by UB3LYP. The contributions of fragments to the "holes" and "electrons" and Inter Fragment Charge Transfer (IFCT) in the electronic excitation process were analyzed by the Ros and Schuit method (C-squared population analysis method, SCPA) in the Multiwfn 3.8 program.

OLEDs Fabrication and Measurement

All the devices were grown on glass substrates pre-coated with a 160-180 nm thick layer of indium tin oxide (ITO) with a sheet resistance of 10 Ω per square. Before loading into the deposition system, the ITO substrates were pre-cleaned carefully and the surface was treated by oxygen plasma for 15 minutes. After UV ozone treatment, hole-injection material HATCN (6 nm) was firstly thermally deposited on, followed by the hole-transporting material HAT-CN (0.2%): TAPC (50 nm), emissive layer 1 (the phosphors doped in the host TCTA, 10 nm), emissive layer 2 (the phosphors doped in 26DCzPPy, 10 nm), and electron-transporting material Tm3PyP26PyB (60 nm). Finally, a cathode composed of lithium fluoride (LiF, 1 nm)/aluminum (Al, 150 nm) was sequentially deposited onto the substrate in the vacuum of 10^{-6} Pa. The current density-voltage-luminance (*J-V-L*) characteristics were measured using a Keithey 2400 Source meter and a Keithey 2000 Source multimeter equipped with a calibrated silicon photodiode. The EL spectra were tested using a brightness light

distribution characteristics measurement system C9920-11. The EQE of the EL device was calculated based on the photo energy examined using the photodiode, the EL spectrum and the current passing through the device. All measurements were carried out at room temperature under ambient conditions.

Tables and Figures

Table S1 The crystallographic data of Ir-dm and Ir-md.

	Ir-dm	Ir-md
Formula	$C_{30}H_{17}F_7IrN_7$	$C_{31}H_{21}F_7IrN_7O$
Formula weight	800.71	832.75
T (K)	200.00(10)	199.99(10)
Wavelength (Å)	Mo 0.71073	Cu 1.54178
Crystal system	monoclinic	monoclinic
Space group	I2/a	C2/c
a (Å)	15.8449(6)	22.4391(11)
b (Å)	10.4597(4)	16.4322(8)
c (Å)	34.0306(13)	17.4014(7)
α (deg)	90	90
β (deg)	95.784(4)	108.645(5)
γ (deg)	90	90
V (Å^3)	5611.3(4)	6079.6(5)
Z	8	8
ρ_{calcd} (g/cm^3)	1.896	1.820
μ (Kα) (mm^{-1})	Mo 4.841	Cu 9.238
F (000)	3088.0	3232.0
Range of transm factors (deg)	4.674-59.216	6.798-133.196
Reflns collected	14992	11590
Unique(R_{int})	6628(0.0446)	5379(0.0504)
R_1 [I > 2s(I)]	0.0365	0.0435
wR_2 (all data)	0.0675	0.1124
GOF on F^2	1.015	1.023

$R_1^a = \Sigma||F_o| - |F_c||/\Sigma F_o|$. $wR_2^b = [\Sigma w(F_o^2 - F_c^2)^2/\Sigma w(F_o^2)]^{1/2}$

Table S2 Selected bond lengths and angles of the two complexes.

Bond length	Ir-dm	Ir-md
Selected	Bond length (Å)	Bond length (Å)
Ir-C(1)	2.004(4)	2.007(6)
Ir-C(2)	2.012(4)	2.025(7)
Ir-N(1)	2.044(3)	2.025(6)
Ir-N(2)	2.045(3)	2.044(6)
Ir-N(3)	2.099(3)	2.095(6)
Ir-N(4)	2.168(4)	2.180(5)
Selected	(°)	(°)
C(1)-Ir-N(1)	80.46(15)	80.2(3)
C(2)-Ir-N(2)	79.99(16)	80.7(3)
N(3)-Ir-N(4)	76.45(13)	76.2(2)

Table S3 The electronic cloud density distribution.

Complex	Orbital	Energy/eV (Calculated)	Energy/eV [a] (experiment)	Composition (%)			
Ir-mm				medfppy	medfppy	Ir	fptz
	HOMO	-5.61	-5.68	21.50	39.37	35.70	3.40
	LUMO	-1.76	-3.02	19.53	2.75	1.90	75.79
Ir-dm				dfbpy	medfppy	Ir	fptz
	HOMO	-5.90	-5.71	10.80	53.12	32.16	3.89
	LUMO	-1.96	-2.94	77.47	2.25	3.29	16.98
Ir-md				dfbpy	medfppy	Ir	fptz
	HOMO	-5.99	-5.69	21.14	35.72	37.82	5.29
	LUMO	-1.92	-2.98	6.29	22.16	1.77	69.77

[a] The experimental energy: E_{HOMO} (eV) = - (E_{ox} - $E_{Fc/Fc+}$ + 4.8) eV; E_{LUMO} (eV) = E_{HOMO} + $E_{bandgap}$; $E_{bandgap}$ = 1240/$\lambda_{abs\text{-}onset}$.

Table S4 NTO results for the iridium(III) complexes based on optimized T_1 geometries.

Complex	NTO	Contribution from Ir center and ligand orbitals to NTOs (%)				Main Contribution for $S_0 \longrightarrow T_1$ transition / E_{cal} / *f*	Assignment
		dfbpy/medfppy	medfppy	Ir	fptz		
Ir-mm	Hole	73.30	4.05	20.87	1.75	H-L (53.50%) / 2.27 eV / 0.00	^{3}LC(78.12%)/^{3}MLCT(13.59%)
	Particle	91.11	1.74	4.45	2.68		
Ir-dm	Hole	2.09	85.41	11.35	1.13	H-L (50.69%) / 2.31 eV / 0.00	^{3}LC(85.55%)/^{3}MLCT(8.90%)
	Particle	1.26	93.63	3.89	1.21		
Ir-md	Hole	2.77	79.11	16.60	1.50	H-L (72.96%) / 2.27 eV / 0.00	^{3}LC(83.90%)/^{3}MLCT(9.90%)
	Particle	2.11	91.07	4.21	2.58		

[a] E_{cal} and *f* denote calculated excitation energy and oscillator strength, respectively. The oscillator strength of $S_0 \rightarrow T_1$ is zero owing to the spin-forbidden character of singlet-triplet transition.

Table S5 The calculated orbital transition analyses for the iridium(III) complexes based on their optimized S_0 geometries

Complex	Main Contribution for $S_0 \longrightarrow S_1$ transition / E_{cal} / *f*	Assignment
Ir-mm	H-L (75.99%) / 3.16 eV / 0.0214	^{1}MLCT(44.86%)/^{1}LLCT(34.82%)/^{1}ILCT(12.54%)
Ir-dm	H-L (85.06%) / 3.21 eV / 0.0137	^{1}MLCT(43.27%)/^{1}LLCT(38.35%)/^{1}ILCT(11.13%)

Ir-md	H-L (61.41%) / 3.34 eV / 0.0281	^{1}MLCT(48.10%)/^{1}LLCT(25.41%)/^{1}ILCT(21.63%)

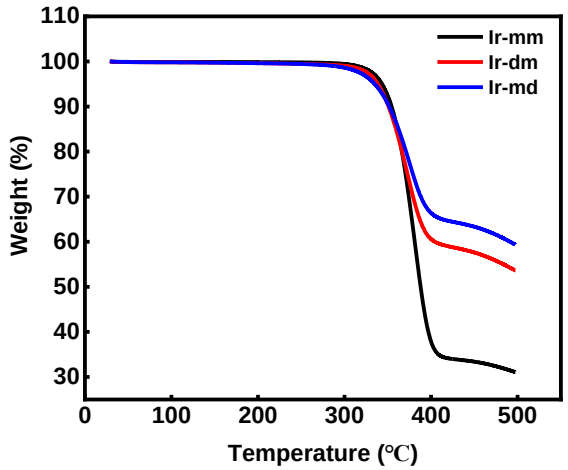

Fig. S1 The TG curves of the three complexes.

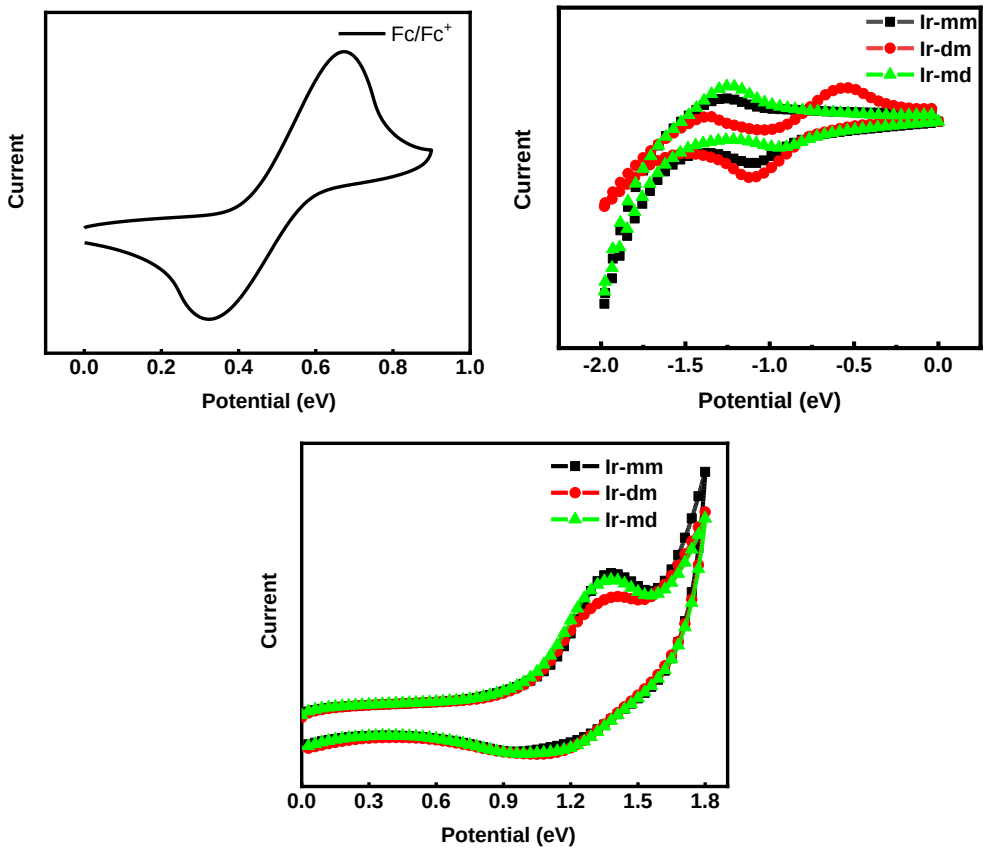

Fig. S2 Cyclic voltammograms of the three iridium(III) complexes and Fc/Fc^+.

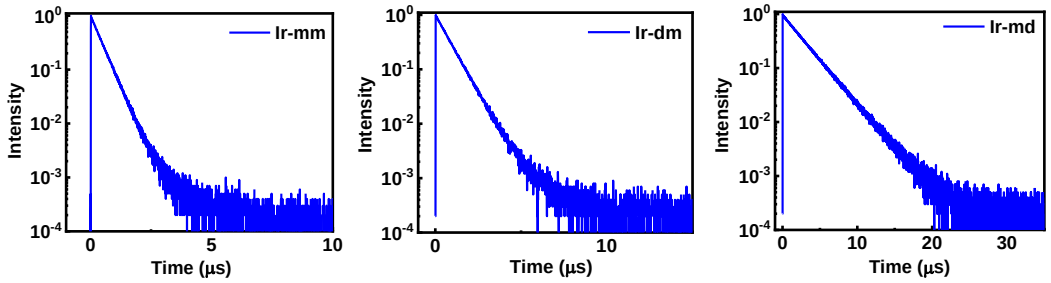

Fig. S3 The lifetime decay curves of the three complexes.

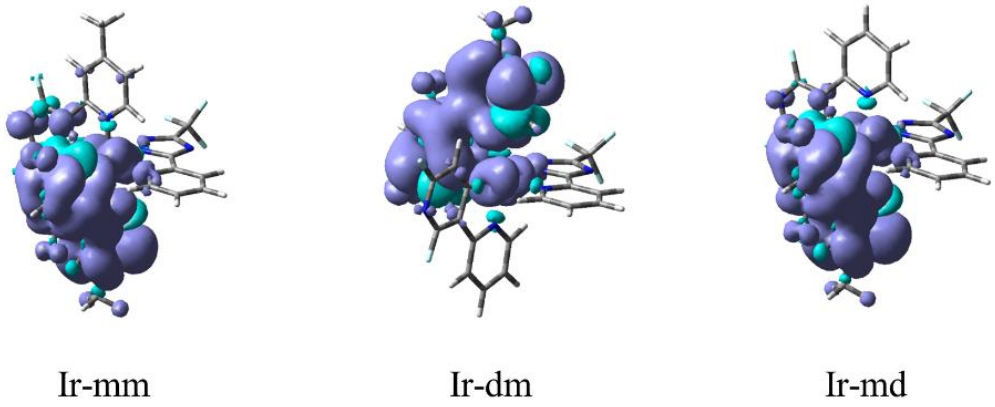

Fig. S4 The spin-density distribution of T_1 state of the three complexes.

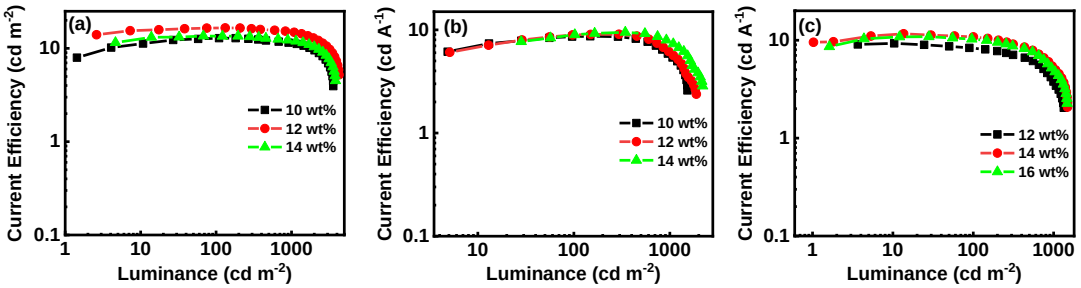

Fig. S5 The current efficiency versus luminance curves with different doped concentration: a) for complex Ir-mm; b) for complex Ir-dm; c) for complex Ir-md.